Surface modification of titanium carbide MXene monolayers (Ti_2C and Ti_3C_2) via chalcogenide and halogenide atoms

ARTICLE TYPE

Cite this: DOI: 10.1039/xxxxxxxxxx

Surface Modification of Titanium Carbide MXenes Monolayers (Ti_2C and Ti_3C_2) via Chalcogenide and Halogenide Atoms

M. Faraji[1], A. Bafekry[2,3,†], M. M. Fadlallah[4], F. Molaei[5], N. N. Hieu[6,7], P. Qian[8], M. Ghergherehchi[9], D. Gogova[10],

Received Date
Accepted Date

DOI: 10.1039/xxxxxxxxxx

www.rsc.org/journalname

Inspired by the recent successful growth of Ti_2C and Ti_3C_2 monolayers, here, we investigate structural, electronic, and mechanical properties of functionalized Ti_2C and Ti_3C_2 monolayers by means of density functional theory calculations. The results reveal that monolayers of Ti_2C and Ti_3C_2 are dynamically stable metals. Phonon band dispersion calculations demonstrate that two-surface functionalization of Ti_2C and Ti_3C_2 via chalcogenides (S, Se, and Te), halides (F, Cl, Br, and I), and oxygen atoms results in dynamically stable novel functionalized monolayer materials. Electronic band dispersions and the density of states calculations reveal that all functionalized monolayer structures preserve the metallic nature of both Ti_2C and Ti_3C_2 except the Ti_2C-O_2, which possesses behavior of an indirect semiconductor via full-surface oxygen passivation. In addition, it is shown that although, halide passivated Ti_3C_2 structures are still metallic, there exist multiple Dirac-like cones around the Fermi energy level, which indicates that semi-metallic behavior can be obtained upon external effects by tuning the energy of the Dirac cones. In addition, the computed linear-elastic parameters prove the functionalization is a powerful tool in tuning the mechanical properties of stiff monolayers of bare Ti_2C and Ti_3C_2. Our study discloses the electronic and structural properties of Ti_2C and Ti_3C_2 MXene monolayers are suitable for surface modification, which is highly desirable for materials properties engineering and device integration.

Inspired by the discovery of graphene[1] and due to its exceptional properties considerable research has been focused on two-dimensional materials (2DMs) including transition metal (TM) dicalcogenides[5], phosphorene[4], hexagonal boron nitrides[2], silicene[3], etc. 2DMs such as graphene[6–8], MoS_2[9], WS_2[10], and boron nitride[11,12] are a type of nanomaterials that have attracted increasing attention in the last decade because of their fascinating properties, which are different from their bulk counterparts[13–16]. Their inherent properties vary from those of their bulk structures due to their atomic thickness. Mechanical or chemical exfoliation and deposition methods are widely used to manufacture these materials[17,18]. Moreover, the quantum containment of electrons in the 2D plane imparts remarkable electrical and electronic characteristics[19–21]. The combination of proper mechanical and physical properties (thermal, electronic, optical) is also of large importance in development of new implementations, where mechanics is combined with condensed matter physics to construct a scalable theoretical structure[22]. In this regard, 2DMs are expected to have a large share in many applications, ranging from energy storage and conversion[23,24] to gas storage or separation[25,26], photocatalysis[27], high-performance sensors[28,29], and membranes[30].

Among the 2DMs MXenes with the chemical formula: $M_{n+1}X_nT_x$ (M = Sc, Ti, V, Cr, Zr, Nb, Mo, Hf, Ta; X = C, N; n = 1-3, T_x=surface termination, e.g., -OH, -F, -O) are genuinely at the frontier of materials science and pledge new scientific and technical horizons[31]. MXenes, a rapidly growing class of 2D multi-layered transition metal carbides and nitrides introduced first by Naguib et al.[32] by discovery of the first two-dimensional (2D) titanium carbide ($Ti_3C_2T_x$). By a process known as inter-

[1] TOBB University of Economics and Technology, Sogutozu Caddesi No 43 Sogutozu, 06560, Ankara, Turkey.
[2] Department of Radiation Application, Shahid Beheshti University, Tehran, Iran.
[3] Department of Physics, University of Antwerp, Groenenborgerlaan 171, B-2020 Antwerp, Belgium.
[4] Department of Mining and Geological Engineering, University of Arizona, Tucson, USA.
[5] Department of Physics, Faculty of Science, Benha University, 13518 Benha, Egypt.
[6] Institute of Research and Development, Duy Tan University, Da Nang 550000, Viet Nam.
[7] Faculty of Natural Sciences, Duy Tan University, Da Nang 550000, Viet Nam.
[8] Department of Physics, University of Science and Technology Beijing, Beijing 100083, China.
[9] Department of Electrical and Computer Engineering, Sungkyunkwan University, 16419 Suwon, Korea. Email: mitragh@skku.edu
[10] Department of Physics, University of Oslo, P.O. Box 1048, Blindern, Oslo, Norway.
† To whom correspondence should be addressed. Email: bafekry.asad@gmail.com

calation, MXenes accommodate different ions and molecules between monolayers, which is often a required step to exploit the material's unique properties and tailor them.[33] Since then, they are used in distinct applications which includes energy conversion and storage[34], electromagnetic interference shielding[35,36], adsorption[37], anti-microbial activity[38,39], membrane[40], reinforcements[41], and catalysis[42]. Besides the aforementioned properties, the MXenes surfaces can be functionalized with different chemical groups such as O, OH, and F, making them a good option for surface state engineering[43].

Computationally, it has been shown that a change in surface termination can change electrical and optical properties. In this regard, several studies have been performed to consider the effect of surface functionalization on thermal transport[44,45], electronic properties[46–49], optical features[50,51], and thermoelectric[52,53], in different types of MXenes. H. Wang et al.[56] reported a hybrid electrode made of 2D NbN nanocrystals and self-assembled $Ti_3C_2T_x$ MXene. The good conductivity and porous nature of NbN monolayers have brought significant advantages for ion infiltration and electrolyte to facilitate, for utilizing in energy storage systems, at a high rate. As a result, NbN-$Ti_3C_2T_x$ electrodes have depicted a thickness independent rate performance, which is much better than the pristine MXene electrode. E. M. D. Siriwardane et al.[57] studied the structural, electronic, stability, ion kinetics, and electrochemical of M_2CS_2 Mxenes functionalized with sulfur (where M is referred to W, Mo, Cr, Ta, Nb, V, Hf, Zr, Ti, and Sc). The sulfur element preferred to seat at different sites, on pristine M_2C Mxenes and constructed a dramatic stable compound. For M_2CS_2 MXene structures with M= Nb, V, Hf, Zr, and Ti elements, full Li coverage attraction has been reported on both surfaces. R. Liu et al.[58] assembled a low-cast, efficient, and simple wearable and flexible pressure sensor using MXene and a piece of woven cotton fabric as the active material and substrate, respectively. The MXene-coated cotton can retain moisture and air permeability perfectly. The pressure sensor has been depicted excellent stability, a relaxation speed and rapid response, and high sensitivity. W. Y. Chen et al.[59] functionalized $Ti_3C_2T_x$ MXene with a superhydrophobic coating layer by utilizing fluoroalkylsilane (FAS) molecules. The analysis methods have demonstrated that the surface properties can be controlled by the functionalized groups.

Q. Zhao et al.[60] investigated $Ti_3C_2T_x$ MXene monolayer to remove uric acid and creatinine from simulated dialysate and aqueous solution. A high chemisorption rate has been reported with larger chemisorption capacity compared to other chemisorption materials like carbon, as a result of hydrophilic surface functionalizations and the open interlayer structure of $Ti_3C_2T_x$, which allow chemisorption between MXene monolayers. The properties of differently synthesized $Ti_3C_2T_x$ MXenes strongly depend upon fluoride and hydroxy/oxyl terminations, which has a higher creatinine chemisorption capacity. In addition to the mentioned research, the interest in 2D MXenes is dramatically increasing since modifying the properties of MXenes by variety of approaches has promoted their application in different fields[61–65].

Stimulated by the approaches described above, we have explored the structural and electronic properties of Ti_2C and Ti_3C_2 monolayers and have investigated the effect of functionalization on them by first-principle calculations. We have found out that 2D Ti_2C and Ti_3C_2 MXenes are promising materials with metallic characteristics, while oxygen passivated Ti_2C monolayer has been shown to possess semiconducting behavior.

1 Method

The density-functional theory (DFT)-based calculations were performed emploing the plane-wave basis projector augmented wave (PAW) method along with the generalized gradient approximation (GGA) in the form of the Perdew-Burke-Ernzerhof (PBE)[66,67] functional as implemented in the Vienna *ab-initio* Simulation Package (VASP)[68,69]. Van der Waals (vdW) correction proposed by Grimme was used to describe the long-range vdW interactions[70]. In addition, charge transfers analysis was accomplished using the Bader technique[71]. The kinetic energy cut-off of 500 eV was set for plane-wave expansion and the energy was minimized between each electronic steps below 10^{-8} eV. In order to get fully-optimized structures, total Hellmann-Feynman forces were reduced to 10^{-7} eV/Å. The integration over the **k**-point mesh was performed using $21 \times 21 \times 1$ Monkhorst-Pack scheme for the primitive unit cell[72]. The PHONOPY code[73] was employed in order to obtain phonon band dispersions based on the small-displacement methodology.

2 Ti_2C and Ti_3C_2 monolayers

The geometric atomic structure, phonon dispersion, electronic band structure with the corresponding density of states (DOS) and partial density of states (PDOS) of Ti_2C and Ti_3C_2 monolayers, are depicted in Figs. 1(a-c) top and bottom, respectively. After optimization, the lattice parameters of Ti_2C and Ti_3C_2 are calcu-

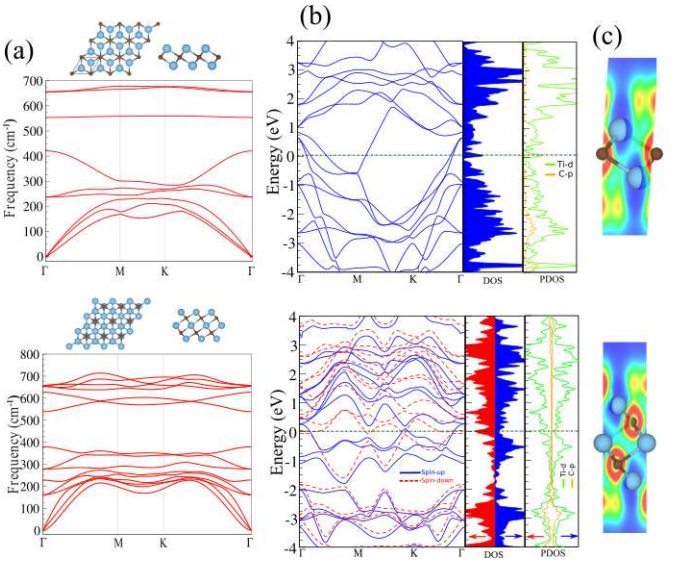

Fig. 1 (a) Phonon spectrum of pristine Ti_2C (top panel) and Ti_3C_2 (bottom of panel). Atomic structure of Ti_2C/Ti_3C_2 monolayer indicated in the top of panel. Azure and brown balls represent the Ti and C atoms, respectively. (b) Electronic structure (b) and PDOS (c) of Ti_2C (top of panel) and Ti_3C_2 (bottom of panel) monolayers. (c) refers to contour plot of the electron localization function (ELF). Red (blue) region denotes high (low) electron density.

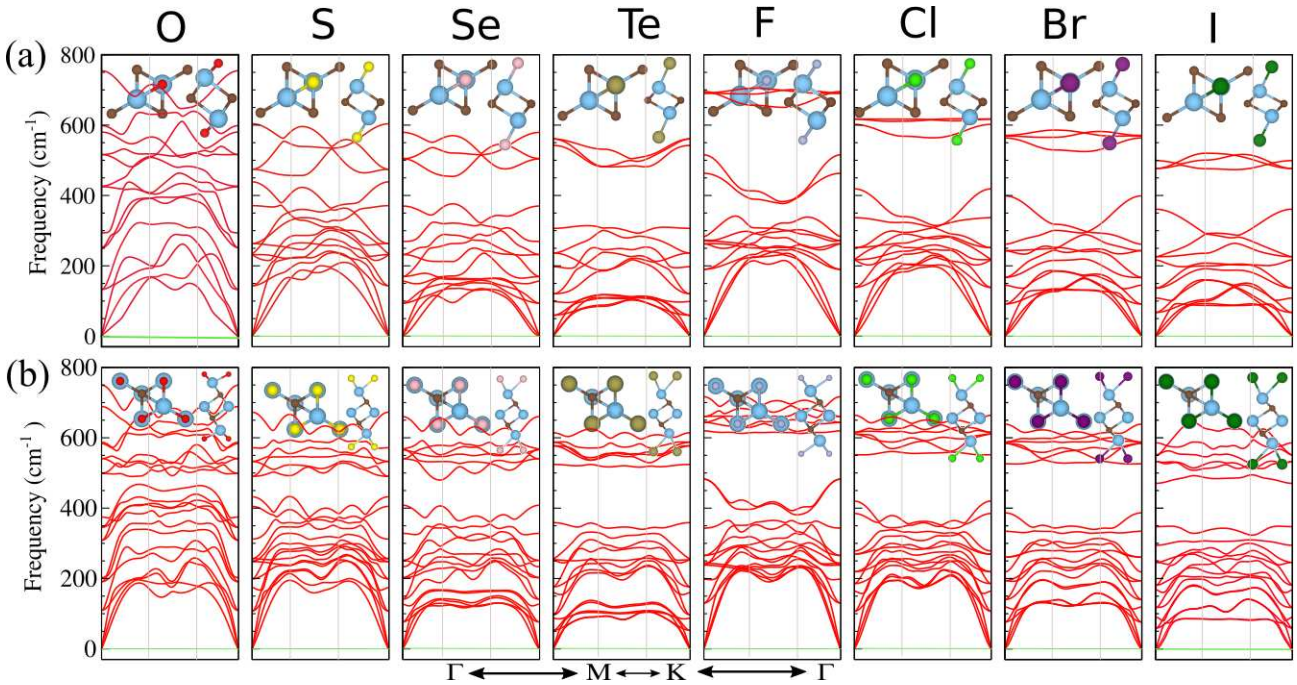

Fig. 2 Phonon spectrum of the functionalized Ti_2C (a) and Ti_3C_2 (b) monolayers. Insets are top and side views of atomic structures of monolayers.

lated to be 3.04 and 3.09 Å, respectively. Notice that, each C atom in the studied structures is covalently bonded with its neighboring Ti atoms, and the bond length of Ti_2C and Ti_3C_2, are found to be 2.10 and 2.21 Å, respectively. The thicknesses of Ti_2C and Ti_3C_2 are calculated to be 2.31 and 4.66 Å, respectively. The calculated lattice parameters, bond lengths and thicknesses of Ti_2C and Ti_3C_2 are in good agreement with the corresponding experimental and theoretical values[74,76–80].

The contour plot of the electron localization function (ELF) are illustrated in Figs. 1(c) top and bottom, respectively. Based on the charge analysis, each Ti atom gains approximately 1.86e from the adjacent C atoms in Ti_2C, while in Ti_3C_2, each Ti atom gains 1.75e from the adjacent C atoms. The charge redistribution within the two monolayers is due to the different electro-negativity of Ti and C atoms -1.54 and 2.54, respectively. The cohesive energy per atom was calculated using the following equation[74]:

$$E_{coh} = (nE_{Ti} + mE_C - E_{MXenes})/N, \quad (1)$$

where E_{Ti} and E_C and E_O represent the energies of isolated single Ti and C atoms, respectively, E_{MXenes} represents the total energy of the MXene. While the n, m and N are the number of Ti, C and total atoms, correspondingly. The cohesive energies of Ti_2C and Ti_3C_2 monolayers are found to be: -0.173 and -0.6 eV/atom, respectively, which indicates that Ti_3C_2 is more favorable than the pristine Ti_2C, which coincides well with previous calculations[74].

The results obtained for the phonon spectra of Ti_2C and Ti_3C_2 monolayers are depicted in Fig. 1(a) which agree with some published spectra[81,82]. For the Ti_2C monolayer, there are nine vibrational modes, including three acoustic modes and six optical modes because its primitive cell contains three atoms. Two of the six optical phonon modes are nondegenerate and two doubly degenerate at the Γ-point. Three acoustic modes are the out-of-plane acoustic (ZA), transverse acoustic (TA), and in-plane longitudinal acoustic (LA) modes. Near the Γ-point, the ZA mode has a quadratic dispersion, while both TA and LA modes possess a linear dispersion. In the case of Ti_3C_2 monolayer, the phonon spectrum has 15 vibrational modes. Only four of 12 optical phonon modes of the Ti_3C_2 are nondegenerate, the rest are degenerate at the Γ point.

In the phonon spectra of both Ti_2C and Ti_3C_2 monolayers, there is a frequency range where both acoustic and optical vibrational modes coexist. The lack of gap between the acoustic and optical modes can cause a strong acoustic-optical scattering, which greatly affects the thermal conductivity of the Ti_2C and Ti_3C_2 monolayers. More importantly, there are no imaginary frequencies in the phonon spectra of both Ti_2C and Ti_3C_2 monolayers. It implies that Ti_2C and Ti_3C_2 monolayers are dynamically stable, so they can be experimentally synthesized as freestanding monolayers. The electronic band structure with the corresponding density of states (DOS) and projected DOS (PDOS) of pristine Ti_2C and Ti_3C_2 monolayers are presented in Fig. 1(b). Our computational results demonstrate that Ti_2C is a metal, while Ti_3C_2 exhibits a ferromagnetic-metal behavior with 1.9 μ_B in the ground state. In both monolayers, the contribution of the orbitals of Ti atoms to the electronic bands, especially above the Fermi level, is dominant. From Fig. 1(b) it can be seen that the contribution of the C atoms orbitals is evident below the Fermi level, in the energy range from -2.5 eV to -4.0 eV for both monolayers. The calculated band structures and DOS/PDOS of Ti_2C and Ti_3C_2 monlolayers are in good agreement with previous reports[74,83–85]. The contour plot of the electron localization function (ELF) is shown in Fig. 1(c). The red and blue regions denote high and low electron density, respectively. The electron density is enriched around

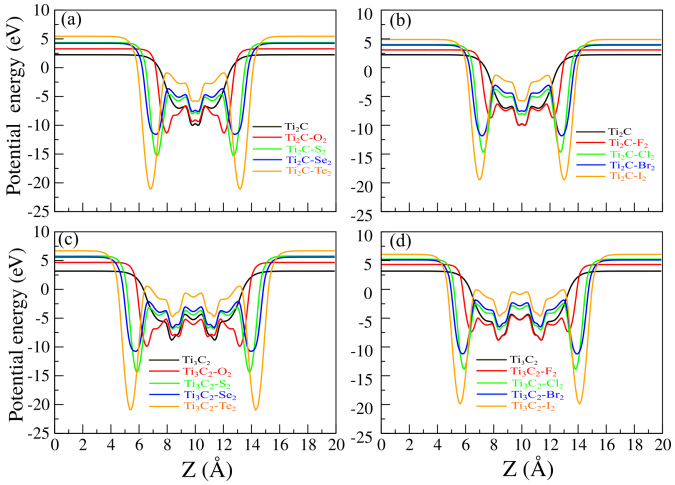

Fig. 3 Potential average of functionalized Ti_2C monolayer with (a) chalcogen and (b) halogen atoms as well as functionalized Ti_3C_2 monolayer with (c) chalcogen and (d) halogen atoms.

the carbon atoms, while there is an electron depletion around the Ti atoms as it is manifested in the inset of Fig. 1(c).

3 Suface functionalization

In the next step, we gain insigh into the chemical functionalization of Ti_2C and Ti_3C_2 monolayers with chalcogen (O, S, Se, and Te) and halogen (F, Cl, Br, and I) atoms. Upon chemical modification, the structure of the systems is significantly altered which may affect even their stability. Tabel I shows the lattice parameters, bond lengths and thicknesses of functionalized Ti_2C-X_2 and Ti_3C_2-X_2 are larger than the corresponding values of Ti_2C and Ti_3C_2, except for X=O, which is in line with some reported results[74,86]. Moreover, the binding energies of functional atoms on both monolayers are calculated using the equation below:

$$E_{bind} = (E_{MXenes} + 2 * E_X - E_{func-MXenes})/2, \quad (2)$$

where E_{MXenes} and $E_{func-MXenes}$ stand for the total energies of bare and functionalized monolayers, while E_X denotes the energies of the isolated atoms.

In Table 1 the computed results for the binding energies of atoms on the surfaces of Ti_2C and Ti_3C_2 monolayers are provided. The calculated E_{bind} of Ti_2C-X_2 and Ti_3C_2-X_2 follow an order of X functionalization O > S > Se > Te and O > F > Cl > Br> I due to the decrease in d_2 (the bond length at the surface). Note, the O atom has the highest binding energy per atom (9.98 and 9.88 eV/atom for Ti_2C and Ti_3C_2 monolayers, respectively). Apparently, except for the F atom, there is a decreasing trend from Ti_2C to Ti_3C_2 indicating the better chemical suitability of the Ti_2C monolayer. As the number of Ti and C atoms increases in the formula of the bare MXene, the occupied orbitals increase and thus, the unoccupied orbitals number decreases and this leads to a slightly lower binding energy of the adatoms.

In Fig. 2, we illustrate the results obtained for the phonon spectra of Ti_2C and Ti_3C_2 after complete chemical modification via the chalcogen and halogen atoms. From Fig. 2, it is obvious that all configurations of the chemically functionalized Ti_2C and Ti_3C_2 with the chalcogen and halogen atoms are dynamically stable because there are no negative frequencies in their phonon spectra. The value of the phonon frequency, especially the frequency of the optical modes, depends strongly on the size of the chalcogen and halogen atoms. The maximum frequency of the optical modes decreases as the chalcogen (halogen) atom changes from O to Te (F to I). In the case of O-termination, the Ti-O bond stretching gives rise to higher optical phonon frequencies at the Γ point. The same holds true in the case of the F-termination, while for the other atoms the highest phonon frequency at the Γ decreases as the atomic radius and mass increases. The phonon bands of Ti_2CO_2, Ti_2CF_2 and $Ti_3C_2O_2$ are similar to some previous studies[87,88].

Fig. 3 presents the results of calculations for the plane-average electrostatic potential of chemically functionalized Ti_2C and Ti_3C_2 with chalcogen and halogen atoms. Due to the symmetrical structure, there is no a difference in the potential between the two sides of these monolayers. The electrostatic potential of all monolayers, including pristine and functionalized Ti_2C and Ti_3C_2 ones, are flat in the vacuum region. Compared to the pristine Ti_2C and Ti_3C_2 monolayers, the potential of functionalized Ti_2C and Ti_3C_2 monolayers are deeper, in which, the potential of functionalized by Te(I) monolayers are the deepest one compared to that of the other chalcogen (halogen) atoms. Also, the depth and the height of the planar part of the potential increases as the electronegativity decreases - see Figs. 3(a-d). The height of the planar electrostatic potential for Ti_3C_2-X_2 is larger than that for the corresponding one of Ti_2C-X_2. We have also calculated the work function Φ of all investigated monolayers and the values obtained are listed in Tab. 1. Note that the Φ refers to the electron's ability to escape from the material surface and can be estimated by the minimum energy for an electron to move from the Fermi and vacuum level. The work function of materials depends strongly on their electron affinity, ionization energy and electronegativity (see table I). The results obtained demonstrate the work function of Ti_2C-X_2 is larger than the corresponding one of Ti_3C_2-X_2. It implies that electrons can more easily escape from the Ti_3C_2-X_2 surface than from the Ti_2C-X_2 ones (see Tab. 1).

3.1 Electronic properties

It is well-known that almost all MXene monolayers are metals and one can turn their electronic properties by surface functionalization. In Fig. 4, we present our computational results for the band structures of the functionalized MXene monolayers with chalcogen and halogen atoms Ti_2C-X_2 and Ti_3C_2-X_2. As expected, Ti_2C becames a semiconductor with an energy gap of 0.25 (1.01) eV at the PBE (HSE06) level after being fully functionalized with oxygen atoms. The band gap value agrees well with previous calculations[82,87]. Ti_2C-O_2 possesses characteristics of an indirect semiconductor with the valence band maximum (VBM) located at the Γ-point and the conduction band minimum (CBM) lying on the MK-path. However, with exception of Ti_2C-O_2, the functionalized Ti_2C-X_2 and Ti_3C_2-X_2 still preserve metallic characteristics after surface functionalization. It is worth mentioning that the Dirac cones are created in Ti_3C_2-X (X=F, Cl, Br, I) at the M and

Table 1 The structural and electronic parameters including lattice constant **a**; Ti-C (d_1) and Ti-X (d_2) bond lengths; Ti-C-Ti [in Ti_2C] and C-Ti-C [in Ti_3C_2] (θ_1) and X-Ti-X (θ_2) bond angles; the thickness layer defined by the difference between the largest and smallest z coordinates of atoms (t)the binding energy per atom, (E_b); the charge transfer from Ti to X atoms (ΔQ); the work function (Φ); the band gap (E_g), and electron affinity (E_a), ionization energy (E_I) and electronegativity (χ) for X atom[75].

	a (Å)	d_1 (Å)	d_2 (Å)	t (Å)	θ_1 (°)	θ_2 (°)	E_b (eV/atom)	Φ (eV)	ΔQ (eV)	E_g (eV)	E_a (eV)	E_I (eV)	χ
Ti_2C-O_2	3.03	2.18	1.97	4.45	92.18	100.16	9.98	5.80	0.97	0.25(1.01)	1.46	13.62	3.44
Ti_2C-S_2	3.18	2.20	2.40	5.52	87.55	83.17	6.83	6.03	0.68	M	2.08	10.36	2.58
Ti_2C-Se_2	3.22	2.20	2.54	5.82	85.93	78.65	6.03	5.39	0.56	M	2.02	9.75	2.55
Ti_2C-Te_2	3.29	2.18	2.82	6.36	82.53	71.18	5.09	4.40	0.43	M	1.97	9.01	2.10
Ti_2C-F_2	3.05	2.10	2.15	4.77	86.91	90.27	7.33	4.93	0.69	M	3.40	17.42	3.98
Ti_2C-Cl_2	3.22	2.15	2.49	5.52	83.32	80.31	5.38	4.64	0.56	M	3.61	12.97	3.16
Ti_2C-Br_2	3.31	2.18	2.63	5.75	81.68	77.83	4.56	4.32	0.51	M	3.36	11.8	2.96
Ti_2C-I_2	3.45	2.23	2.82	6.02	79.12	75.49	3.46	3.81	0.56	M	3.05	10.45	2.66
Ti_3C_2-O_2	3.03	2.15 (2.19)	1.97	6.98	90.46	100.18	9.88	6.12	0.97	M	1.46	13.62	3.44
Ti_3C_2-S_2	3.14	2.20 (2.17)	2.39	8.04	89.04	81.79	6.76	6.15	0.65	M	2.08	10.36	2.58
Ti_3C_2-Se_2	3.14	2.21 (2.14)	2.56	8.37	89.05	76.22	5.96	5.29	0.53	M	2.02	9.75	2.55
Ti_3C_2-Te_2	3.21	2.24 (2.12)	2.84	8.91	88.56	68.74	5.01	4.15	0.41	M	1.97	9.01	2.10
Ti_3C_2-F_2	3.07	2.18 (2.07)	2.16	7.20	90.77	90.39	7.33	4.84	0.69	M	3.40	17.42	3.98
Ti_3C_2-Cl_2	3.18	2.22 (2.11)	2.49	7.97	88.70	79.11	5.34	4.50	0.56	M	3.61	12.97	3.16
Ti_3C_2-Br_2	3.24	2.24 (2.12)	2.62	8.21	87.81	76.11	4.46	4.11	0.52	M	3.36	11.8	2.96
Ti_3C_2-I_2	3.33	2.29 (2.15)	2.49	8.49	86.46	72.81	3.18	3.56	0.42	M	3.05	10.45	2.66

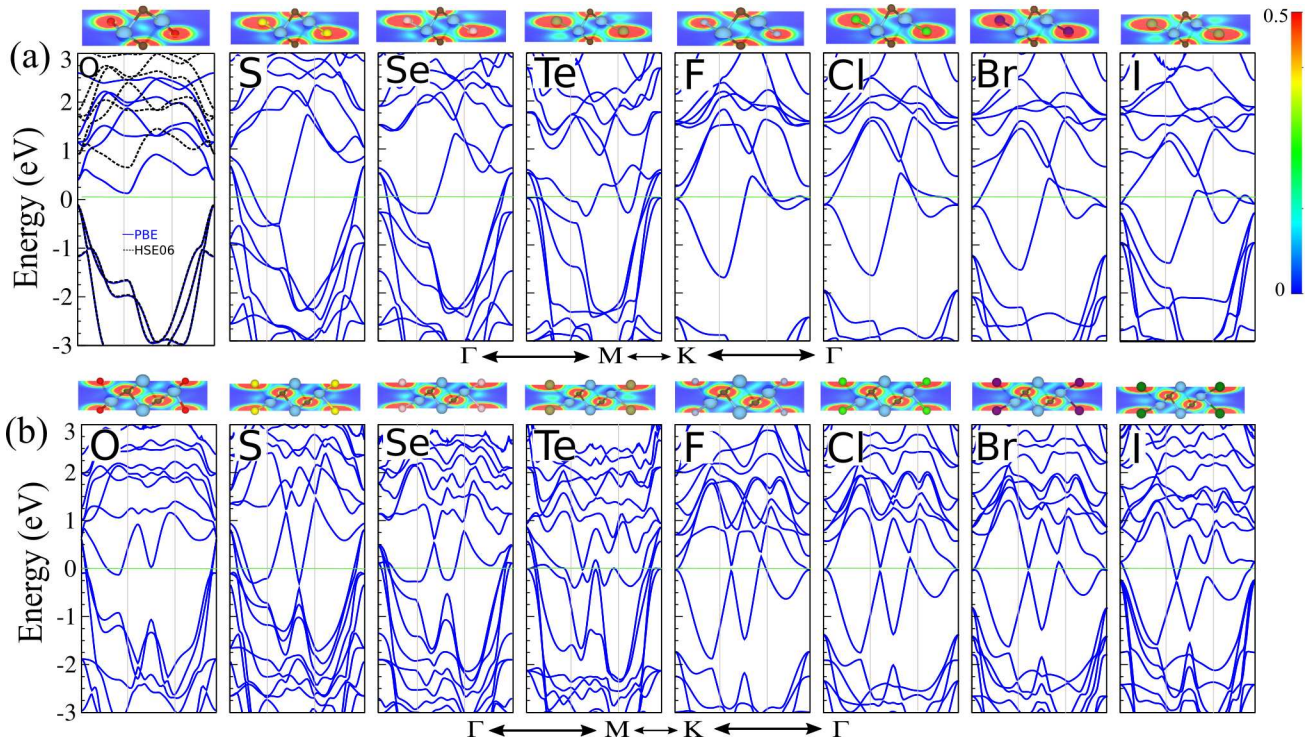

Fig. 4 Electronic band structure of functionalized Ti_2C (top) and Ti_2CO_2 (bottom) monolayers. Corresponding DOS and PDOS, indicated in top of electronic band structures. Zero of energy is set at the Fermi energy.

K points as shown in the corresponding band structures around the Fermi energy. Therefore, the semi-metallic behavior can be obtained upon external fields by tuning the energy of the Dirac cones.

To clearly see the nature and contribution of atomic orbitals to the formation of electronic bands of the functionalized MXene monolayers, we have also calculated the PDOS of the functionalized monolayers as depicted in Fig. 5. Focusing on the case of Ti_2C-O_2, we can see that the p-orbitals of Ti atoms contribute greatly to the formation of electronic bands, especially in the conduction band. Besides, the contribution of the C-p orbital to the electronic band, especially the valence band, is significant. As illustrated in Fig. 5(a), in the high energy region of the valence band, from -4 eV to -6 eV, the contribution of C-p orbital is

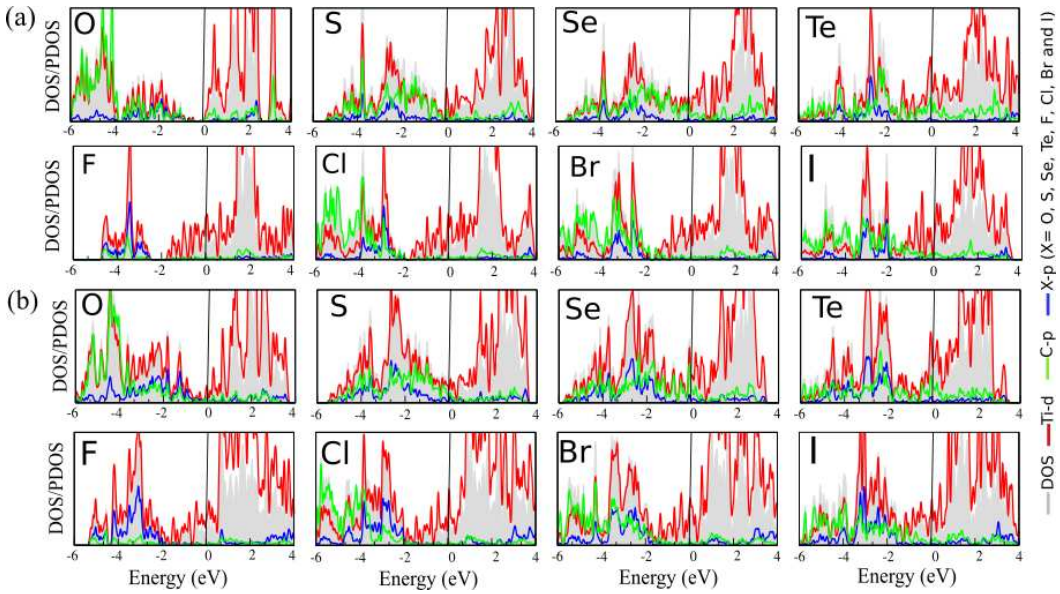

Fig. 5 DOS and PDOS of functionalized Ti_2C (top) and Ti_3C_2 (bottom) monolayers. Zero of energy is set at the Fermi energy.

more dominant than that of other atomic orbitals, including Ti-*p* orbital. From the PDOS in Fig. 5(a), we can see that opening the band gap of Ti_2C-O_2 could be caused by the hybridization of *d*-orbital of carbon atoms and *p*-orbital of oxygen atoms. For the other configurations, the contribution of Ti-*d* orbitals to the formation of electronic bands is distinctly prominent, that is similar to the case of Ti_2C-O_2. In addition, the *p*-orbital of atom X atoms also contributes significantly to the electronic bands, especially the valence band. The Ti orbitals are dominating at the Fermi energy with a considerable contribution of C orbitals in the cases of X=S, Se and Te. The Ti_2C-Te_2 monolayer has a metallicity character more than Ti_2C-S_2 and Ti_2C-Se_2 monolayers due to its number of electrons. The band structures and DOS/PDOS of Ti_2C-X_2 (X=S, Se, Te) are in good agreement with published in a previous theoretical study[86]. For halogen atoms (X=F, Cl, Br, I),Fig. 5(a), the contribution of C orbitals at the Fermi energy is very small as compared to the chalcogen atoms (X=S, Se, Te). The DOS/PDOS of Ti_3C_2-X_2 is very similar to the corresponding DOS/PDOS of Ti_2C-X_2 (Fig. 5(b)). In addition, the contribution of X=F, Cl, Br and Cl orbitals in Ti_3C-X_2 monolayer is larger than the corresponding contribution in the Ti_2C-X_2 monolayer.

3.2 Mechanical properties

Using the harmonic approximation, we explore the linear-elastic properties of the proposed monolayers in terms of their in-plane stiffnes and Poisson's ratio values. The in-plane stiffness is known as the measure of the rigidity of a 2D material. For the bare monolayers of Ti_2C and Ti_3C_2, the elastic constants are isotropic and the in-plane stiffness values are found to be 130 N/m and 231 N/m, respectively, which correspond well with a previous study[85]. This indicates that increasing the number of C and Ti layers in the monolayer structure increases the stiffness of the materials. After surface functionalization, it is found that halide atoms increase the stiffness, while Se and Te chalcogenides weaken the rigidity of the monolayer. Apparently, the highest in-plane stiffness is calculated for oxygen-saturated monolayers (272 and 375 N/m for Ti_2C and Ti_3C_2, correspondingly). As the atomic radius increases from O to Te, in-plane stiffness possesses a decreasing trend in both monolayers. In addition, a similar trend is found when Ti_2C and Ti_3C_2 monolayers are saturated with halide atoms. Notably, the fluorinated and oxygenated monolayers of Ti_3C_2 are stiff materials with in-plane stiffness values comparable to that of graphene (340 N/m). As a result, it is important to mention that surface functionalization of Ti_2C and Ti_3C_2 can tune their elastic properties depending on the type of

Table 2 The elastic parameters of bare and functionalized monolayers; the in-plane stiffness, C; and Poisson's ratio, ν)).

	C (N/m)	ν
Ti_2C	130	0.23
Ti_2C-O_2	272	0.31
Ti_2C-S_2	176	0.24
Ti_2C-Se_2	89	0.20
Ti_2C-Te_2	17	0.93
Ti_2C-F_2	220	0.31
Ti_2C-Cl_2	177	0.27
Ti_2C-Br_2	177	0.25
Ti_2C-I_2	167	0.22
Ti_3C_2	231	0.17
Ti_3C_2-O_2	375	0.29
Ti_3C_2-S_2	267	0.27
Ti_3C_2-Se_2	161	0.59
Ti_3C_2-Te_2	78	0.80
Ti_3C_2-F_2	349	0.25
Ti_3C_2-Cl_2	294	0.24
Ti_3C_2-Br_2	294	0.24
Ti_3C_2-I_2	276	0.22

adatoms. On the other hand, we calculate the Poisson's's ratio, which is defined as the ratio of the transverse contraction strain to the longitudinal extension, and the results are presented in Table 2. Our results for the Poisson's ratio of bare Ti_2C and Ti_3C_2 monolayers are: 0.23 and 0.17, respectively, i.e., these values are close to that of graphene (0.16) due to the presence of C atoms in the structures. It is found out that as the atomic mass of the halide atom increases from F to I, the Poisson's ratio decreases for both structures. In contrast, as the atomic mass of the chalcogenide atom from S to Te increases, the Poisson's ratio values are found to increase due to less mechanical stability of the functionalized monolayer. In both monolayers of Ti_2C and Ti_3C_2, the Te-functionalized structures exhibit a very high Poisson's ratio values, which are still in the 2D limit. The high Poisson's ratios of these monolayers indicate the high flexibility of the monolayers along the unstretched direction.

4 Conclusion

We have investigated the structural, electronic, and mechanical properties of functionalized Ti_2C and Ti_3C_2 monolayers by means of ab-initio calculations. Our results revealed that monolayers of Ti_2C and Ti_3C_2 are dynamically stable metalic structures. Phonon band dispersion calculations showed the two-surface functionalization of Ti_2C and Ti_3C_2 via chalcogenides (S, Se, and Te), halides (F, Cl, Br, and I), and oxygen atoms results in dynamically stable novel functionalized monolayer materials. Electronic band dispersions and the corresponding density of states calculations have indicated that all the functionalized monolayer structures preserve the metallic nature of both Ti_2C and Ti_3C_2 except for Ti_2C-O_2, which possessess an indirect semiconductor behavior via full-surface oxygen passivation. Moreover, it has been shown that although, halide passivated Ti_3C_2 structures are still metallic, there exist multiple Dirac-like cones around the Fermi-level, which indicates that semi-metallic behavior can be obtained upon external effects by tuning the energy of the Dirac cones. Moreover, the calculated linear-elastic parameters indicated that the functionalization plays a crucial role in tuning the mechanical properties of stiff monolayers of bare Ti_2C and Ti_3C_2. This theoretical study opens a new door for exploration and will stimulate further experimental research on these exciting materials in future.

5 Conflicts of interest

The authors declare that there are no conflicts of interest regarding the publication of this paper.

6 Acknowledgments

This work was supported by the National Research Foundation of Korea grant funded by the Korea government (NRF-2015M2B2A4033123).

References

1 K. S. Novoselov, A. K. Geim, S. V. Morozov, D. Jiang, Y. Zhang, S. V. Dubonos, I. V. Grigorieva, and A. A. Firsov, Electric field effect in atomically thin carbon films, Sci., 306, 666âĂŞ669, 2004.

2 D. Pacile, J. C. Meyer, C. O. Girit, and A. Zettl, The two-dimensional phase of boron nitride: Few-atomic-layer sheets and suspended membranes, Appl. Phys. Lett., 92, 133107, 2008.

3 B. Lalmi, O. Hamid, H. Enriquez, A. Kara, S. Vizzini, B. Ealet, and B. Aufray, Epitaxial growth of a silicene sheet, Appl. Phys. Lett., 97, 223109, 2010.

4 H. Liu, T. N. Adam, Zh. Zhen, Zh. Luo, X. Xu, D. Tomanek, and P. D. Ye. Phosphorene: an unexplored 2D semiconductor with a high hole mobility, ACS Nano, 8, 4033-4041, 2014.

5 C. Ataca, H. Sahin, and S. Ciraci, Stable, single-layer MX_2 transition-metal oxides and dichalcogenides in a honeycomb-like structure, J. Phys. Chem. C, 116, 8983-8999, 2012.

6 Y. Dong, Z.-S. Wu, W. Ren, H.-M. Cheng, and X. Bao, Graphene: A Promising 2D Material for Electrochemical Energy Storage, Sci. 62, 724-40 2017.

7 V. Berry, Impermeability of graphene and its applications, Carbon N. Y., 62, 1-10, 2013.

8 K. Einalipour Eshkalak, S. Sadeghzadeh, and F. Molaei, CâĂŕ: Physical Processes in Nanomaterials and Nanostructures Interfacial Thermal Resistance Mechanism for Polyaniline (C_3N)-Graphene Heterostructure, J. Phys. Chem. C, 2020.

9 A. Bafekry, C. Stampfl, and M. Ghergherehchi, Strain, electric-field and functionalization induced widely tunable electronic properties in MoS_2/BC_3,/C_3N and/van der Waals heterostructures, Nanotechnol., 31, 295202, 2020.

10 X. Li and H. Zhu, Two-dimensional MoS_2: Properties, preparation, and applications, J. Mater., 1, 33-44, 2015.

11 C. Cong, J. Shang, Y. Wang, and T. Yu, Optical properties of 2D semiconductor WS_2, Adv. Opt. Mater., 6, 1, 1700767, 2018.

12 H. Tan, Y. Fan, Y. Zhou, Q. Chen, W. Xu, and J. H. Warner, Ultrathin 2D photodetectors utilizing chemical vapor deposition grown WS_2 with graphene electrodes, ACS Nano, 10, 8, 7866-7873, 2016.

13 A. Bafekry, M. Faraji, M. M Fadlallah, B. Mortazavi, A. A. Ziabari, A. B. Khatibani, Ch. V. Nguyen, M. Ghergherehchi, D. Gogova, Point Defects in a Two-Dimensional $ZnSnN_2$ Nanosheet: A First-Principles Study on the Electronic and Magnetic Properties, J. Phys. Chem. C 125 , 13067-13075, 2021.

14 A. Bafekry, M. Yagmurcukardes, B. Akgenc, M. Ghergherehchi, B. Mortazavi, First-principles investigation of electronic, mechanical and thermoelectric properties of graphene-like XBi (X= Si, Ge, Sn) monolayers Phys. Chem. Chem. Phys. 23, 12471-12478, 2021.

15 A. Bafekry, C. Stampfl, M. Faraji, M. Yagmurcukardes, M.M. Fadlallah, H.R. Jappor, M. Ghergherehchi, S.A.H. Feghhi, A Dirac-semimetal two-dimensional BeN_4: Thickness-dependent electronic and optical properties Appl. Phys. Lett. 118 , 203103, 2021.

16 M. Faraji, A. Bafekry, D. Gogova, D.M. Hoat, M. Ghergherе-

hchi, Ch. V. Chuong, S.A.H. Feghhi, Novel two-dimensional ZnO_2, CdO_2 and HgO_2 monolayers: a first-principles-based prediction, N. J. Chem. 45, 9368-9374, 2021.

17 M. Khazaei, M. S. Bahramy, N. S. Venkataramanan, H. Mizuseki, and Y. Kawazoe, Chemical engineering of prehydrogenated C and BN-sheets by Li: Application in hydrogen storage, J. Appl. Phys., 106, 94303, 2009.

18 L. Ci, L. Song, Ch. Jin, D. Jariwala, D. Wu, Y. Li, A. Srivastava, Z. F. Wang, K. Storr, and L. Balicas, Atomic layers of hybridized boron nitride and graphene domains, Nat. Mater., 9, 430-435, 2010.

19 H. Wang, J. T. Robinson, X. Li, and H. Dai, Solvothermal reduction of chemically exfoliated graphene sheets, J. Am. Chem. Soc., 131, 9910-9911, 2009.

20 R. Ibragimova, M. J. Puska, and H.-Komsa, pH-Dependent Distribution of Functional Groups on Titanium-Based MXenes, ACS Nano, 13, 9171-9181, Aug. 2019.

21 M. M. Fadlallah, A. A. Maarouf, U. Schwingenschlogl, U. Eckern, Unravelling the interplay of geometrical, magnetic and electronic properties of metal-doped graphene nanomeshes, J. Phys.: Condens. Matter 29, 055301 2017.

22 W. Zhang, D. Chang, Q. Gao, Ch. Niu, Ch. Li, F. Wang, X. Huang, C. Xia, and Y. Jia, Interlayer coupling and external electric field tunable electronic properties of a 2D type-I tellurene/MoS_2 heterostructure, J. Mater. Chem. C, 6, 10256-10262, 2018.

23 D. M. Hoat, T. V Vu, M. M. Obeid, and H. R. Jappor, Tuning the electronic structure of 2D materials by strain and external electric field: case of GeI_2 monolayer, Chem. Phys., 527, 110499, 2019.

24 D. Akinwande, Ch. J. Brennan, J. S. Bunch, Ph. Egberts, J. R. Felts, H. Gao, R. Huang, J.-S. Kim, T. Li, and Y. Li, A review on mechanics and mechanical properties of 2D materials-Graphene and beyond, Extrem. Mech. Lett., 13, 42-77, 2017.

25 R. Kumar, E. Joanni, R. K. Singh, D. Singh, and S. A. Moshkalev, Recent advances in the synthesis and modification of carbon-based 2D materials for application in energy conversion and storage, Prog. Energy Combust. Sci., 67, 115-157, 2018.

26 L. Tang, X. Meng, D. Deng, and X. Bao, Confinement catalysis with 2D materials for energy conversion, Adv. Mater., 31, 1901996, 2019.

27 X. Zhang, L. Hou, A. Ciesielski, and SamorÃň, 2D materials beyond graphene for highâĂŘperformance energy storage applications, Adv. Energy Mater., 6, 1600671, 2016.

28 Y. Peng, Y. Li, Y. Ban, and W. Yang, TwoâĂŘDimensional Metal-Organic Framework Nanosheets for MembraneâĂŘBased Gas Separation, Angew. Chemie, 129, 9889-9893, 2017.

29 A. K. Singh, K. Mathew, H. L. Zhuang, and R. G. Hennig, Computational screening of 2D materials for photocatalysis, J. Phys. Chem. Lett., 6, 1087-1098, 2015.

30 R. Irshad, K. Tahir, B. Li, Z. Sher, J. Ali, and S. Nazir, A revival of 2D materials, phosphorene: Its application as sensors, J. Ind. Eng. Chem., 64, 60-69, 2018.

31 S. Feng, Z. Lin, X. Gan, R. Lv, and M. Terrones, Doping two-dimensional materials: ultra-sensitive sensors, band gap tuning and ferromagnetic monolayers, Nanoscale Horizons, 2, 72-80, 2017.

32 L. Prozorovska and R. Kidambi, StateâĂŘofâĂŘtheâĂŘArt and Future Prospects for Atomically Thin Membranes from 2D Materials, Adv. Mater., 30, 1801179, 2018.

33 J. L. Hart, K. Hantanasirisakul, A. C. Lang, B. Anasori, D. Pinto, Y. Pivak, J. Tijn van Omme, S. J. May, Y. Gogotsi, M. L. Taheri, Control of MXenesâĂŹ electronic properties through termination and intercalation, Nat Commun 10, 522 (2019).

34 M. Khazaei, A. Ranjbar, M. Arai, T. Sasaki, and S. Yunoki, Electronic properties and applications of MXenes: a theoretical review, J. Mater. Chem. C, 5, 2488-2503, 2017.

35 M. Naguib et al., Two-dimensional nanocrystals produced by exfoliation of Ti_3AlC_2, Adv. Mater., 23, 4248-4253, 2011.

36 J. Luo, X. Tao, J. Zhang, Y. Xia, H. Huang, L. Zhang, Y. Gan, Ch. Liang, and W. Zhang, Sn4 ion decorated highly conductive Ti_3C_2 MXene: promising lithium-ion anodes with enhanced volumetric capacity and cyclic performance, ACS Nano, 10, 2, 2491-2499, 2016.

37 F. Shahzad, M. Alhabeb, Ch. B. Hatter, B. Anasori, S. M. Hong, Ch. M. Koo, and Y. Gogotsi, Electromagnetic interference shielding with 2D transition metal carbides (MXenes), Sci., 353, 1137-1140, 2016.

38 J. Liu, H. B. Zhang, R. Sun, Y. Liu, Zh. Liu, A. Zhou, and Zh. Zh. Yu, Hydrophobic, Flexible, and Light weight MXene Foams for High-Performance Electromagnetic-Interference Shielding, Adv. Mater., 29, 1-6, 2017.

39 J. Zhu, E. Ha, G. Zhao, Y. Zhou, D. Huang, G. Yue, L. Hu, N. Sun, Y. Wang, and L. Y. S. Lee, Recent advance in MXenes: A promising 2D material for catalysis, sensor and chemical adsorption, Coord. Chem. Rev., 352, 306-327, 2017.

40 F. Alimohammadi, M. Sharifian Gh, N. H. Attanayake, A. C. Thenuwara, Y. Gogotsi, B. Anasori, and D. R. Strongin, Antimicrobial properties of 2D MnO_2 and MoS_2 nanomaterials vertically aligned on graphene materials and Ti_3C_2 MXene, Langmuir, 34, 7192-7200, 2018.

41 K. Rasool, M. Helal, A. Ali, C. E. Ren, Y. Gogotsi, and K. A. Mahmoud, Antibacterial activity of $Ti_3C_2T_x$ MXene, ACS Nano, 10, 3, 3674-3684, 2016.

42 R. Pandey, K. Rasool, V. E. Madhavan, B. Aissa, Y. Gogotsi, and K. A. Mahmoud, Ultrahigh-flux and fouling-resistant membranes based on layered silver/MXene ($Ti_3C_2T_x$) nanosheets, J. Mater. Chem. A, 6, 8, 3522-3533, 2018.

43 M. Khazaei, A. Ranjbar, M. Ghorbani-Asl, M. Arai, T. Sasaki, Y. Liang and S. Yunoki, Nearly free electron states in MXenes, Phys. Rev. B, 2016, 93, 205125.

44 X. Sheng, Y. Zhao, L. Zhang, and X. Lu, Properties of two-dimensional Ti_3C_2 MXene/thermoplastic polyurethane nanocomposites with effective reinforcement via melt blending, Compos. Sci. Technol., 181, 107710, 2019.

45 G. Gao, A. OMullane, and A. Du, 2D MXenes: a new family

of promising catalysts for the hydrogen evolution reaction, ACS Catal., 7, 494-500, 2017.

46 Z. Hemmat, P. Yasaei, J. F. Schultz, L. Hong, L. Majidi, A. Behranginia, L. Verger, N.Jiang, M. W. Barsoum, and R. F. Klie, Tuning thermal transport through atomically thin $Ti_3C_2T_x$ MXene by current annealing in vacuum, Adv. Funct. Mater., 29, 19, 1805693, 2019.

47 S. Sarikurt, D. CakÄśr, M. Keceli, and C. Sevik, The influence of surface functionalization on thermal transport and thermoelectric properties of MXene monolayers, Nanoscale, 10, 8859-8868, 2018.

48 M. Khazaei, M. Arai, T. Sasaki, Ch.-Y. Chung, N. S. Venkataramanan, M. Estili, Y. Sakka, and Y. Kawazoe, Novel Electronic and Magnetic Properties of Two-Dimensional Transition Metal Carbides and Nitrides, Adv. Funct. Mater., 23, 2185-2192, 2013.

49 J. L. Hart, K. Hantanasirisakul, A. C. Lang, B. Anasori, D. Pinto, Y. Pivak, J. T. v. Omme, Steven J. May, Y. Gogotsi, and M. L. Taheri. Control of MXenes electronic properties through termination and intercalation, Nat. Commun., 10, 1, 2019.

50 G. R. Berdiyorov, Effect of surface functionalization on the electronic transport properties of Ti_3C_2 MXene, Epl, 111, 6, 2015.

51 S. Li, J. He, Nachtigall, L. Grajciar, and F. Brivio, Control of spintronic and electronic properties of bimetallic and vacancy-ordered vanadium carbide MXenes via surface functionalization, Phys. Chem. Chem. Phys., 21, 25802-25808, 2019.

52 G. R. Berdiyorov, Optical properties of functionalized $Ti_3C_2T_2$ (T= F, O, OH) MXene: First-principles calculations, Aip Adv., 6, 5, 55105, 2016.

53 H. Xu, A. Ren, J. Wu, and Z. Wang, Recent Advances in 2D MXenes for Photodetection, Adv. Funct. Mater., 2000907, 2020.

54 H. Kim, B. Anasori, Y. Gogotsi, and H. N. Alshareef, Thermoelectric Properties of Two-Dimensional Molybdenum-Based MXenes, Chem. Mater., 29, 6472-6479, 2017.

55 S. Kumar and U. Schwingenschlogl, Thermoelectric performance of functionalized Sc_2C MXenes, Phys. Rev. B, 94, 35405, 2016.

56 H. Wang, J. Li, X. Kuai, L. Bu, L. Gao, X. Xiao and Y. Gogotsi, Enhanced rate capability of ion-accessible $Ti_3C_2T_x$-NbN hybrid electrodes, Adv. Energy Mater. 2020,10, 2001411.

57 E. M. D. Siriwardane, I. Demiroglu, C. S., F. M. Peeters, and D. Cakir, Assessment of sulfur-functionalized MXenes for Li-ion battery applications, J. Phys. Chem. C, 1932-7447, 2020.

58 L. Rui, L. Jianmin, L. Meng, Z. Qinghong, S. Guoying, L. Yaogang, H. Chengyi , and W. Hongzhi, A MXene-coated air permeable pressure-sensing fabric for smart wear, ACS Appl. Mater. Interfaces, 1944-8244, 2020.

59 W. Y. Chen, S. Lai, C. Yen, X. Jiang, D. Peroulis, and L. A. Stanciu, Surface functionalization of TiCT MXene with highly reliable superhydrophobic protection for volatile organic compounds sensing, ACS Nano, 14, 11490-11501, 2020.

60 Q. Zhao, M. Seredych, E. Precetti, C. E. Shuck, M. Harhay, R. Pang, C. Shan, and Y. Gogotsi, Adsorption of uremic toxins using $Ti_3C_2T_x$ MXene for dialysate regeneration, ACS Nano 14, 11787-11798, 2020.

61 A. Bafekry, M. Faraji, D.M. Hoat, M. Shahrokhi, M.M. Fadlallah, F. Shojaei, S. A. H. Feghhi, M. Ghergherehchi, D. Gogova, $MoSi_2N_4$ single-layer: a novel two-dimensional material with outstanding mechanical, thermal, electronic and optical properties, J. Phy. D: Appl. Phys., 54, 155303, 2021.

62 A. Bafekry, B. Akgenc, M. Ghergherehchi, F.M. Peeters, Strain and electric field tuning of semi-metallic character $WCrCO_2$ MXenes with dual narrow band gap, J. Phys. Conde. Matter 32 (25), 355504, 2021.

63 A. Bafekry, C.V. Nguyen, C. Stampfl, B. Akgenc, M. Ghergherehchi, Oxygen Vacancies in the Single Layer of Ti_2CO_2 MXene: Effects of Gating Voltage, Mechanical Strain, and Atomic Impurities physica status solidi (b), 2000343, 2021.

64 A. Bafekry, M. Faraji, M.M. Fadlallah, A.B. Khatibani, A. abdolahzadeh Ziabari, M. Ghergherehchi, Sh. Nedaei, S. Farjami Shayesteh, D. Gogova, Tunable electronic and magnetic properties of $MoSi_2N_4$ monolayer via vacancy defects, atomic adsorption and atomic doping, Appl. Surf. Sci. 559, 149862, 2021.

65 A Bafekry, C Stampfl, Band-gap control of graphenelike borocarbonitride g-BC_6N bilayers by electrical gating, Phys. Rev. B 102, 195411, 2021.

66 J. P. Perdew, K. Burke, and M. Ernzerhof, Generalized gradient approximation made simple, Phys. Rev. Lett. 77, 3865, 1996.

67 J. P. Perdew, K. Burke, and M. Ernzerhof, Generalized gradient approximation made simple, Phys. Rev. Lett. 78, 1396, 1997.

68 G. Kresse and J. Hafner, Ab initio molecular dynamics for liquid metals, Phys. Rev. B 47, 558, 1993.

69 G. Kresse and J. Hafner, Efficient iterative schemes for ab initio total-energy calculations using a plane-wave basis set, Phys. Rev. B 49, 14251, 1994.

70 S. J. Grimme, Semiempirical GGA-type density functional constructed with a long-range dispersion correction, Comput. Chem. 27, 1787, 2006.

71 G. Henkelman, A. Arnaldsson, and H. Jonsson, A fast and robust algorithm for Bader decomposition of charge density, Comput. Mater. Sci. 36, 354, 2006.

72 H.J. Monkhorst and J.D. Pack, Special points for Brillouin-zone integrations, Phys. Rev. B 13, 12, 1976.

73 D. Alfe, PHON: A program to calculate phonons using the small displacement method, Comput. Phys. Commun. 180, 2622, 2009.

74 N. Zhang, Y. Hong, S. Yazdanparast, M. Asle Zaeem, Superior structural, elastic and electronic properties of 2D titanium nitride MXenes over carbide MXenes: a comprehensive

first principles study, 2D Mater. 5, 045004, 2018.
75 James, Arthur M and Lord, Mary P, Macmillan's Chemical and Physical Data, Macmillan, Basingstoke, 1992.
76 Q. Wan , S. Li and J. Liu , First-Principle Study of Li-Ion Storage of Functionalized Ti_2C Monolayer with Vacancies, ACS Appl. Mater. Interfaces 10 ,6369, 2018.
77 M. Sternik and U. D. Wdowik, Probing the impact of magnetic interactions on the lattice dynamics of two-dimensional Ti_2X (X = C, N) MXenes, Phys. Chem. Chem. Phys. 20 , 7754, 2018.
78 P. Lv, Y.-L Li and J.-F. Wang, Monolayer Ti_2C MXene: manipulating magnetic properties and electronic structures by an electric field Phys. Chem. Chem. Phys. 22, 11266, 2020.
79 O. Mashtalir, M. Naguib, V.N. Mochalin, Y. DallâĂŹAgnese, M. Heon, M.W. Barsoum, Y. Gogotsi, Intercalation and delamination of layered carbides and carbonitrides, Nat. Commun. 4, 1716, 2013.
80 C. Shi, M. Beidaghi, M. Naguib, O. Mashtalir, Y. Gogotsi, and S. J.âĂŁL. Billinge, Structure of Nanocrystalline Ti_3C_2 MXene Using Atomic Pair Distribution Function, Phys. Rev. Lett. 112, 125501, 2020.
81 U. Yorulmaz, ÌĞI. Demiroglu, D. Cakir, O. Gulseren, and Cem Sevik, A systematical ab-initio review of promising 2D MXenemonolayers towards Li-ion battery applications, J. Phys. Energy 2, 032006, 2020.
82 H. Zhang, G. Yang, X. Zuo, H. Tang, Q. Yangaand, G. Li, Computational studies on the structural, electronicand optical properties of graphene-like MXenes(M_2CT_2, M=Ti, Zr, Hf; T=O, F, OH) and their potential applications as visible-light, driven photocatalysts, J. Mater. Chem. A 4, 12913, 2016.
83 Y. Xie, P. R. C. Kent, Hybrid density functional study of structural and electronic properties of functionalized $Ti_n + 1X_n$ (X=C, N) monolayers, Phys. Rev. B 87, 235441, 2013.
84 M. Khazaei, A. Ranjbar, M. Arai, T.o Sasaki, S. Yunoki, Electronic properties and applications of MXenes: a theoretical review, J. Mater. Chem. C 5, 2488, 2017.
85 S. Wang, J.-X. Li, Y.-L. Du, C. Cui, First-principles study on structural, electronic and elastic properties of graphene-like hexagonal Ti_2C monolayer, Computational Materials Science 83, 290, 2014
86 D. Li, X. Chen, P. Xiang, H. Du, B. Xiao, Chalcogenated-Ti_3C_2 MXene (X = O, S, Se and Te) as a high-performance anode material for Li-ion batteries, Applied Surface Science 501, 144221, 2020.
87 A. N. Gandi, H. N. Alshareef, U. Schwingenschlogl, Thermoelectric Performance of the MXenes M_2CO_2 (M = Ti, Zr, or Hf), Chem. Mater. 28, 1647 2016.
88 L. Li, Lattice dynamics and electronic structures of Ti_3 C_2 O_2 and Mo_2 TiC_2 O_2 (MXenes): The effect of Mo substitution, Comput. Mater. Sci. 124, 8 2016.